PHYSICAL REVIEW A **92**, 060701(R) (2015)

Plasmon-mediated electron emission from the coronene molecule under fast ion impact

Shubhadeep Biswas and L. C. Tribedi*
Tata Institute of Fundamental Research, Homi Bhabha Road, Colaba, Mumbai 400 005, India
(Received 21 August 2015; published 7 December 2015)

The existence of the collective electronic excitation in polycyclic aromatic hydrocarbon (PAH) molecules has been predicted before on the basis of the presence of a large delocalized π electron cloud around the carbon skeleton. Here, we present a manifestation of energy and angular distributions of electron emission upon deexcitation of the collective plasmon resonance in coronene, a PAH molecule, under fast ion impact. The angular distributions of these electrons show an unusually enhanced forward-backward angular asymmetry, in contrast to the observed uniform distributions for simpler atomic (Ne) or molecular (CH_4) targets. A simple model of photoelectron angular distribution from an oscillating dipolar plasmon, calculated including the first retardation term in the transition matrix element, provides excellent agreement with the observed distribution. The ratio of forward-to-backward electron emission intensity clearly exhibits a broad peak which is in excellent agreement with the theoretical prediction of the plamson peak. This observation may provide some new inputs towards the astrophysical problem of UV photon absorption by PAHs in the interstellar medium, or in the search for materials suitable for UV plasmonics.

DOI: 10.1103/PhysRevA.92.060701 PACS number(s): 34.50.Fa, 34.50.Gb, 36.40.−c

Polycyclic aromatic hydrocarbon (PAH) molecules are of great interest in recent times because of their astrophysical relevance as well as technological importance. Their unique electronic structure draws the attention of researchers from diverse fields. PAHs consist of fused benzenoid rings of sp^2-hybridized C atoms with a requisite number of H atoms attached to the periphery. The remaining electron from each C atom forms a delocalized π-electron cloud over the C skeleton. For these large π-electron systems, it is expected to show multiparticle collective excitation like plasmon resonance, which is quite familiar in the case of metals [1] or in nuclear reactions [2]. It is possible through a coherent mixer of many single particle excitation states [3,4]. A similar kind of state for fullerenes was realized earlier as the collective oscillation of delocalized π and σ electrons against the ionic cage [5–10]. In general, the experimental detection of such collective state for the PAH molecules is relatively difficult because of its low oscillator strength compared to fullerenes. Moreover, the involvement of multiparticle description makes it hard to tackle theoretically. Because of these difficulties, PAHs are not explored much in this regard, although there were predictions of plasmon excitations around 17 eV [4,11,12]. Recently, the *ab initio* time-dependent density functional theory (TDDFT) as well as the model approach based on the plasmon resonance approximation have also confirmed it [13]. This energy region is assigned to the $\pi + \sigma$ plasmon resonance. In the lower energy region, the existence of π plasmon resonance has also been predicted [13,14].

Apart from their fundamental molecular physics importance, the confirmation of such plasmon resonance can also shed light on the problems related to the other fields of physics. In recent times, it is speculated that there is a large abundance of PAHs in the interstellar medium (ISM) [15] and several unidentified astrophysical features are resultant of electronic excitations of these molecules [16–19]. But there are still some open questions regarding definite assignments to these individual features. According to the "PAH hypothesis," emission of IR photon is caused by deexcitation of PAHs initially pumped by UV photon, which results in the interstellar extinction curve [18,20,21]. The mechanism of UV photon absorption by PAHs is still to be understood fully. Recently, the famous 217.5 nm (5.7 eV) extinction bump on that curve is assigned to the π plasmon excitation in dehydrogenated coronene and its cations [22]. The strong lower wavelength features (below about $\lambda \sim 170$ nm) are still not properly assigned to specific molecular excitations. In this regard, the plasmon resonance structure around 17 eV ($\lambda \sim 73$ nm) may be related to the production mechanism of these deep-UV absorption features, which are primarily responsible for the unidentified IR emissions [23].

From another viewpoint, PAH physics can have a strong overlap with plasmonics, very similar to graphene. Nanoplasmonics research has traditionally used different metals, which constrain their operation to the visible or IR spectral regions. But in recent days, it is extending into the UV region, which could open up possibilities of new applications such as devising sensors for detecting UV resonances taking place in different biological systems, etc. Researchers are continuously engaged in searching for new materials for that [24–26]. In this regard, PAH can be a very good choice, because of its plasmonic feature in the UV region. Moreover, its tunablity, easily achieved by chemical changes, makes it suitable for better plasmonic devices, which can cover a wide spectral range [14].

In the present work, which is a study of energy and angular distributions of electron emission from any PAH molecule under ion impact, the primary aim is to investigate the induced multiparticle collective excitation. The use of highly charged ions ensures a strong perturbation which helps to excite the plasmon efficiently. In addition, charge particles, i.e., cosmic rays, are an inseparable component of the ISM. Photon-induced studies of PAHs have continued for several decades [27,28]. But, ion impact studies are relatively much rarer in literature. Only recently, some studies concentrating on post collision recoil-ion yield measurements [29–32] or the projectile energy loss [33–35] have been

*Corresponding author: lokesh@tifr.res.in

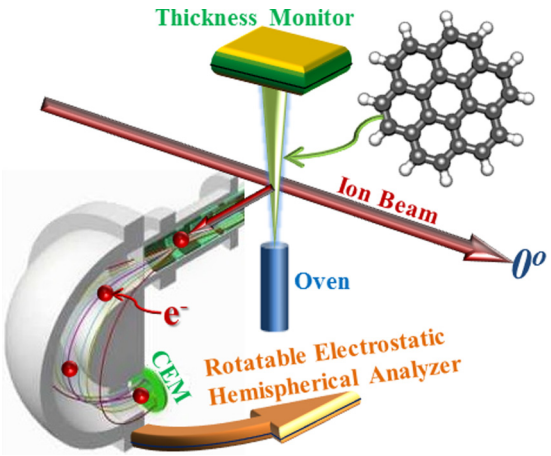

FIG. 1. (Color online) Schematic diagram of the experimental setup [37].

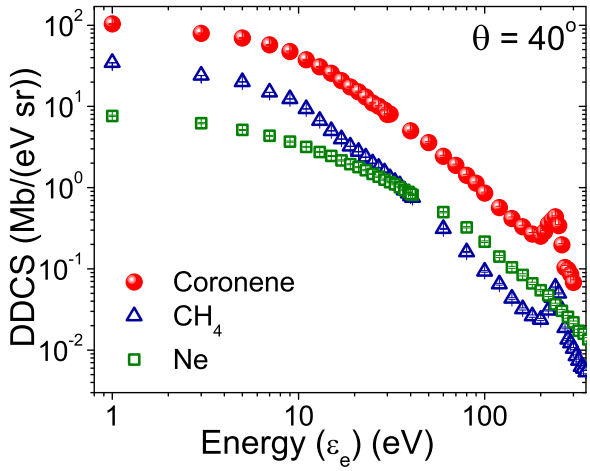

FIG. 2. (Color online) Energy distributions of electron DDCS for coronene (circle), CH_4 (triangle), and Ne (square) targets for emission angle 40°.

reported. On the other hand, to the best of our knowledge, there are hardly any reports of the measurement of post collision differential electron distribution from any PAH molecule, though it can provide crucial information regarding different electronic processes. Particularly for studying plasmon excitation, the electron emission channel is more favorable because it is the fastest mode of deexcitation of this resonance [1].

Here we report the measurement of the absolute double differential cross section (DDCS) of electron emission from a coronene ($C_{24}H_{12}$) molecule under the impact of 3.75 MeV/u bare oxygen ions obtained from the Pelletron accelerator at TIFR, Mumbai. For such high projectile energies the electron capture cross sections are much lower compared to those for the ionization. The two electron processes, such as the double ionization or double capture, etc., are also less probable. The ions were made incident on an effusive vapor jet, prepared by heating 99% pure coronene powder at approximately 200 °C. The fluctuations in the vapor yield were monitored in real time using a quartz crystal based thickness monitor *in situ*. The emitted electrons were energy analyzed and detected by an electrostatic hemispherical analyzer of energy resolution about 6% and a channel electron multiplier detector, respectively [36]. The schematic diagram of the experimental setup is shown in Fig. 1. To put the cross sections in an absolute scale, we employed a self-normalization technique which compares the total carbon *K-LL* Auger cross section for coronene with the absolute value of that measured for the CH_4 target (see [9,38] for details). To check the spectrometer performance, particularly in the low energy part of the spectrum, the same measurements were performed for the Ne and CH_4 targets. Total uncertainty in the absolute cross section data for coronene was estimated to be about 10%–15%, which arises mainly from the target density fluctuation, normalization procedure and the statistical uncertainty.

In Fig. 2, the energy distributions of the absolute DDCS for coronene, CH_4, and Ne targets are shown for the ejection angle $\theta = 40°$. As per convention, 0° is regarded as the forward-most angle along which the ion beam travels. For coronene, the DDCS falls off rapidly as electron energy increases. In general, the qualitative behavior is very similar to the cases of the other two targets and is expected from a simple picture of Coulombic interaction between the active electron and the ionic projectile. In the higher energy range, at around 240 eV, the C *K-LL* Auger electron peak is observed.

The angular distributions of the DDCS for coronene and CH_4 targets are shown in Figs. 3(a)–3(d) for four different electron energies. At lower energies (e.g., 1, 9, and 11 eV) for coronene, the distributions steeply fall off with increasing value of ejection angle. This behavior is in sharp contrast to that obtained for the CH_4 target, for which it is nearly a flat distribution with a little hump at the intermediate angles gradually pronounced with increasing energy. In particular, the associated forward-backward angular asymmetry is noted to be much higher for coronene compared to the CH_4. This

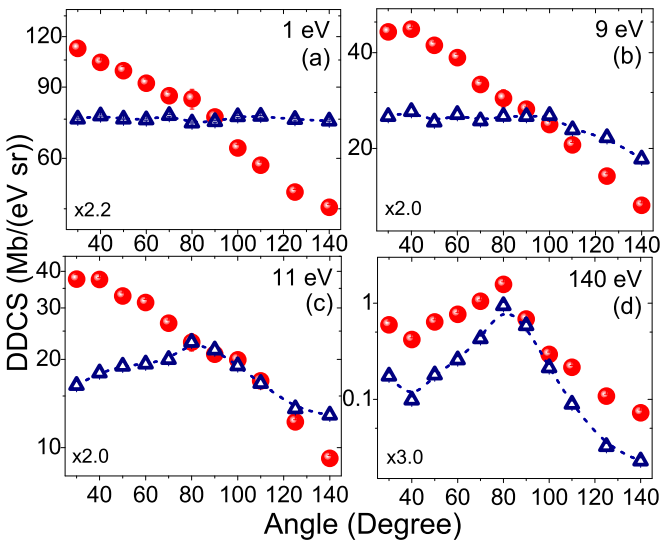

FIG. 3. (Color online) Angular distribution of DDCS for coronene (circle) and CH_4 (triangle) at four different electron energies. The number written at the left bottom corner in each plot is the division factor to get absolute DDCS for CH_4.

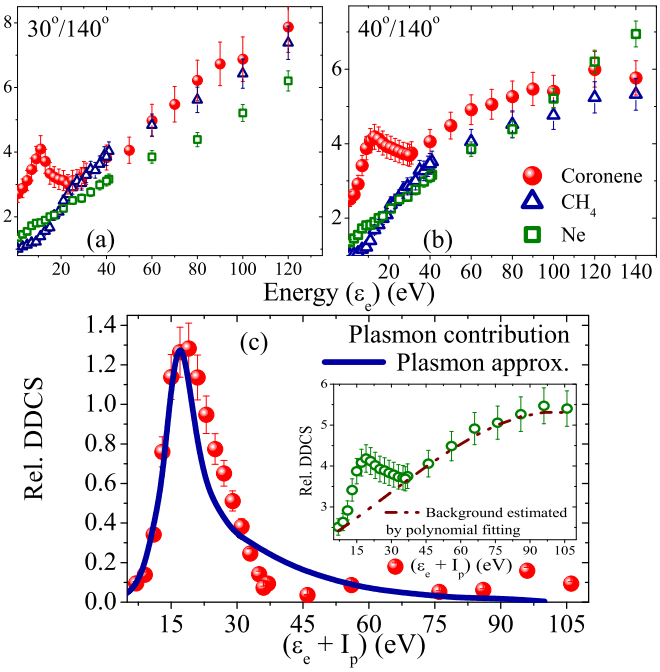

FIG. 4. (Color online) (a) and (b) Energy distributions of relative DDCS [i.e., DDCS (30°)/DDCS (140°) and (40°)/DDCS (140°), respectively] for different targets. (c) Relative DDCS corresponding to only the plasmon contribution for coronene as a function of excitation energy (see text). The solid line represents the plasmon resonance approximation calculation [13]. In the inset the estimated Coulomb background is shown by dashed-dot-dot line.

large discrepancy in angular asymmetry is also observed for other low energy electrons up to around 35 eV, with the maximum at around 10 eV. The observed behavior for CH_4 is very similar to that obtained generally in ion-atom collisions [39]. Normally, the low energy electrons are produced in large impact parameter collisions. As a result, the projectile ion has a minimal effect on the active electron. Their emission is mainly governed by the target Compton profile, which is commonly called the target center effect. It leads to an isotropic electron distribution. As energy increases, the signature of binary collision and projectile post collision interaction become prominent at the intermediate and extreme angles, respectively. But here, clearly this simple ion-atom collision picture is inadequate to explain the observed behavior for coronene in the low energy region. On the other hand, at higher energies, the angular distributions (e.g., 140 eV) corresponding to both the targets are qualitatively very similar. Mainly the binary nature of collision and the projectile post collision effect are manifested. Now, it is to be noted that the predicted $\pi + \sigma$ plasmon energy for coronene is around 17 eV. The electrons ejected following the deexcitation of plasmon will have an energy equal to $\hbar\omega_{\text{plasmon}} - I_p \sim 10$ eV, since the ionization potential (I_p) is 7.29 eV (first) for coronene (in gas phase). As a result, we expect the signature of plasmon electrons at around 10 eV, which is exactly the energy region where the unusual behavior of the angular distribution is found.

To show the above results more precisely, in Figs. 4(a) and 4(b), we plot the energy distributions of "relative DDCS," which is a measure of forward-backward angular asymmetry. Here, a clear difference is visible between the coronene and the other two targets. For Ne and CH_4 targets, the distributions are monotonically increasing with increasing energy, whereas for coronene it gives rise to a prominent broad peak around 10 eV. After that it shows the usual increasing behavior in the higher energy region, similar to the other two targets. Clearly, there is a high degree of angular asymmetry associated with the electron distribution in the predicted plasmon energy region for coronene, in contrast to the cases of the other simpler targets for which any kind of collective excitation is not expected. Since the Coulomb ionization contribution is almost isotropic at these low energies, the enhanced ratio (i.e., the peak around 10 eV) can be considered as a measure of plasmon contribution over Coulomb ionization. It can be extracted by subtracting the continuous Coulomb background. In Fig. 4(b), the plasmon contribution is plotted as a function of excitation energy which is calculated by adding the I_p to the ejected electron energy (ε_e). The background was estimated by fitting a polynomial to the continuum data above 37 eV [see the inset in Fig. 4(b)]. To have a qualitative understanding, the experimentally estimated plasmon contribution is compared with the theoretical calculation of photoionization intensity (normalized at one point) for coronene, estimated by Verkhovtsev *et al.*, within the plasmon approximation formalism [13]. These authors demonstrated that the TDDFT also gives a very similar plasmon peak. Due to the unavailability of proper calculation in the DDCS level for ion interaction, the present comparison between the calculated intensity and the relative DDCS is only to establish the important qualitative features of the plasmon peak, such as peak position and width. The peak position observed experimentally matches very well with the predicted one. The measured width is also approximately the same as that given by the calculation as well as that measured in photoabsorption [12]. The little discrepancy in the higher energy region could be due to the artifact of background subtraction. Here the theoretically predicted π plasmon peaks are not shown. Earlier, this model calculation was seen to reproduce the experimental data for fullerene plasmon quite well [13,40].

To understand the underlying physics mechanism that can give rise to the observed angular distribution in the plasmon energy region, in Fig. 5, we have reanalyzed the distributions around the plasmon peak, i.e., 9–11 eV by a model approach. Similar behavior was observed for other nearby energies. The plasmon excitation can be viewed as the collective oscillation of the polarized electron cloud against the C skeleton. As coronene is a planer molecule and oriented randomly during the experiment, the directions of polarization for different molecules upon interaction with the ionic projectile would be random. We can model the electron emission from the deexcitaion of these oscillations as the photoelectron emission from randomly oriented targets. For ion-induced plasmon excitation, the probability of plasmon excitation reaches its maximum when the impact parameter of the collision is comparable to the dimension of the molecular electron cloud, i.e., in peripheral collisions, as explicitly shown for C_{60} [41,42]. In those peripheral collisions, as the effective momentum transfer would be large, the estimation of the photoelectron angular distribution would require higher

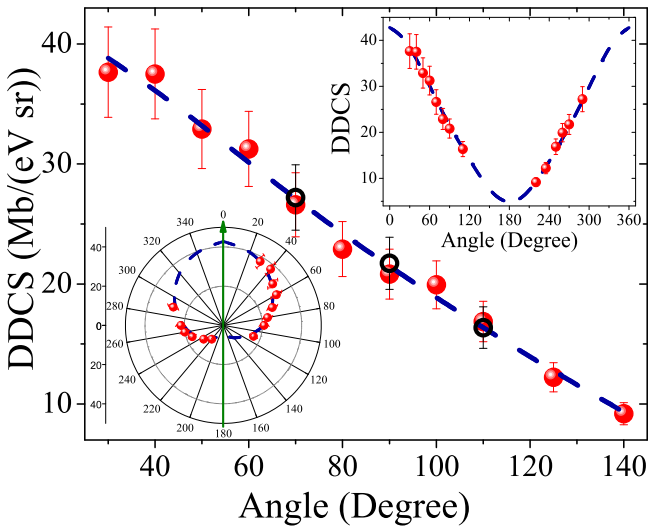

FIG. 5. (Color online) Angular distribution of the DDCS at 11 eV. The dashed line represents the model of photoelectron distribution. The open circles represent the data of corresponding mirror symmetric angles. Insets: Same distributions over the entire 2π angular range in normal as well as polar plots.

order corrections over the dipole approximation during the calculation of transition matrix element. In fact, it has been explicitly shown earlier that for charged particle impact, the contribution of the nondipole term compared to the dipole one is relatively much bigger [43]. In the present case, we have used the photoelectron angular distribution calculated taking into account up to the first-retardation term in the transition matrix element. The distribution is given by [44,45]

$$I(\theta) = 1 - \frac{\beta}{2} P_2(\cos\theta) + \left(\frac{\gamma}{2}\sin^2\theta + \delta\right)\cos\theta, \qquad (1)$$

where along with the dipole anisotropy parameter β, the nondipolar contributions are characterized by another two parameters γ and δ, the quantity θ being the angle of electron emission with respect to the beam direction. The values of these fitting parameters are found to be -0.134, -0.351, and 0.866, respectively. The figure shows that it reproduces the experimental data very well. In the insets we have plotted the distribution in the full angular range. Though the reflection symmetry of the distribution around the beam axis is quite obvious, we have verified it by acquiring data at both sides of the ion beam direction. There are three data points at 70°, 90°, and 110° which can be compared with the values at their corresponding mirror symmetric angles, i.e., 290°, 270°, and 250°, respectively. Their mutual agreements are quite good, which is seen in the main plot. The overall experimentally observed distribution in the entire 2π angular range, and its good agreement with the model clearly indicate the essential qualitative features. In simple terms, without plasmon we expect a flat angular distribution mainly governed by the target center effect. The oscillatory character of the plasmon poses the anisotropic behavior due to the efficient coupling of the strong ionic perturbation of nondipolar nature.

In conclusion, we have experimentally demonstrated the existence of the collective $(\sigma + \pi)$ plasmon resonance in the coronene molecule through the measurement of energy and angular distributions of electrons emitted during the fast ion collisions. The observed anisotropic angular distribution, which is incompatible with the expected isotropic distribution, could be explained by a model based on photoelectron emission from plasmon oscillation, calculated considering up to the first-retardation term in the transition matrix element. The forward-backward angular asymmetry distribution shows a prominent peak due to the plasmon excitation exactly at the expected energy. The plasmon resonance approximation and the TDDFT calculations show excellent agreement with it. Here the plasmon peak is detected explicitly, through the electron emission channel, for a molecule belonging to the PAH family. Apart from the fact that it is an important input to the knowledge of fundamental molecular physics, this result may also enrich our understanding about the UV absorption mechanism of PAHs in the ISM and provides a promising material for UV plasmonics.

The authors would like to acknowledge the Pelletron accelerator staff for the smooth running of the machine during the experiment, D. Misra and S. Kasthurirangan for useful discussions, and Nilesh Mhatre for assistance during the experiments.

[1] F. Calvayrac, P. G. Reinhard, E. Suraud, and C. A. Ullrich, Phys. Rep. **337**, 493 (2000).
[2] K. A. Brueckner and R. Thieberger, Phys. Rev. Lett. **4**, 466 (1960).
[3] H. Gutfreund and W. A. Little, Chem. Phys. Lett. **2**, 589 (1968).
[4] H. Gutfreund and W. A. Little, J. Chem. Phys. **50**, 4478 (1969).
[5] G. F. Bertsch, A. Bulgac, D. Tománek, and Y. Wang, Phys. Rev. Lett. **67**, 2690 (1991).
[6] U. Kadhane, D. Misra, Y. P. Singh, and Lokesh C. Tribedi, Phys. Rev. Lett. **90**, 093401 (2003).
[7] S. W. J. Scully, E. D. Emmons, M. F. Gharaibeh, R. A. Phaneuf, A. L. D. Kilcoyne, A. S. Schlachter, S. Schippers, A. Müller, H. S. Chakraborty, M. E. Madjet, and J. M. Rost, Phys. Rev. Lett. **94**, 065503 (2005).
[8] P. Bolognesi, L. Avaldi, A. Ruocco, A. Verkhovtsev, A. V. Korol and A. V. Solov'yov, Eur. Phys. J. D **66**, 254 (2012).
[9] A. H. Kelkar, L. Gulyás, and Lokesh C. Tribedi, Phys. Rev. A **92**, 052708 (2015).
[10] P. Wopperer, P. M. Dinha, P. G. Reinhard, and E. Suraud, Phys. Rep. **562**, 1 (2015).
[11] Y. Ling and C. Lifshitz, Chem. Phys. Lett. **257**, 587 (1996).
[12] H. W. Jochims, E. Rühl, H. Baumgärtel, S. Tobita, and S. Leach, Int. J. Mass Spectrom. Ion Phys. **167**, 35 (1997).
[13] A. V. Verkhovtsev, A. V. Korol, and A. V. Solov'yov, J. Phys.: Conf. Ser. **490**, 012159 (2014).
[14] A. Manjavacas, F. Marchesin, S. Thongrattanasiri, P. Koval, P. Nordlander, D. Sánchez-Portal, and F. J. G. de Abajo, ACS Nano **7**, 3635 (2013).

[15] Th. Henning and F. Salama, Science **282**, 2204 (1998).
[16] A. Léger and L. d'Hendecourt, Astron. Astrophys. **146**, 81 (1985).
[17] L. J. Allamandola, D. M. Hudgins, and S. A. Sandford, Astrophys. J. **511**, L115 (1999).
[18] A. G. G. M. Tielens, Rev. Mod. Phys **85**, 1021 (2013).
[19] E. L. O. Bakes and A. G. G. M. Tielens, Astrophys. J. **427**, 822 (1994).
[20] J. L. Puget and A. Leger, Annu. Rev. Astron. Astrophys. **27**, 161 (1989).
[21] L. J. Allamandola, A. G. G. M. Tielens, and J. R. Barker, Astrophys. J. Suppl. Ser. **71**, 733 (1989).
[22] W. W. Duley, Astrophys. J. **639**, L59 (2006).
[23] M. S. Robinson, L. W. Beegle, and T. J. Wdowiak, Astrophys. J. **474**, 474 (1997).
[24] J. M. McMahon, G. C. Schatz, and Stephen K. Gray, Phys. Chem. Chem. Phys. **15**, 5415 (2013).
[25] J. Y. Ou, J. K. So, G. Adamo, A. Sulaev, L. Wang, and N. I. Zheludev, Nat. Commun. **5**, 5139 (2014).
[26] A. M. Watson, X. Zhang, R. A. de la Osa, J. M. Sanz, F. González, F. Moreno, G. Finkelstein, J. Liu, and H. O. Everitt, Nano Lett. **15**, 1095 (2015).
[27] R. Boschi, E. Clar, and W. Schmidt, J. Chem. Phys. **60**, 4406 (1974).
[28] P. M. Mishra, L. Avaldi, P. Bolognesi, K. C. Prince, R. Richter, and U. R. Kadhane, J. Phys. Chem. A **118**, 3128 (2014).
[29] A. I. S. Holm, H. Zettergren, H. A. B. Johansson, F. Seitz, S. Rosén, H. T. Schmidt, A. Lawicki, J. Rangama, P. Rousseau, M. Capron, R. Maisonny, L. Adoui, A. Méry, B. Manil, B. A. Huber, and H. Cederquist, Phys. Rev. Lett. **105**, 213401 (2010).
[30] J. Postma, S. Bari, R. Hoekstra, A. G. G. M. Tielens and T. Schlathölter, Astrophys. J. **708**, 435 (2010).
[31] A. Lawicki, A. I. S. Holm, P. Rousseau, M. Capron, R. Maisonny, S. Maclot, F. Seitz, H. A. B. Johansson, S. Rosén, H. T. Schmidt, H. Zettergren, B. Manil, L. Adoui, H. Cederquist, and B. A. Huber, Phys. Rev. A **83**, 022704 (2011).
[32] G. Reitsma, H. Zettergren, L. Boschman, E. Bodewits, R. Hoekstra, and T. Schlathölter, J. Phys. B: At., Mol. Opt. Phys. **46**, 245201 (2013).
[33] E. R. Micelotta, A. P. Jones, and A. G. G. M. Tielens, Astron. Astrophys. **526**, A52 (2011).
[34] E. R. Micelotta, A. P. Jones, and A. G. G. M. Tielens, Astron. Astrophys. **510**, A36 (2010).
[35] P. M. Mishra, J. Rajput, C. P. Safvan, S. Vig, and U. Kadhane, J. Phys. B: At., Mol. Opt. Phys. **47**, 085202 (2014).
[36] D. Misra, K. V. Thulasiram, W. Fernandes, A. H. Kelkar, U. Kadhane, A. Kumar, Y. P. Singh, L. Gulyás, and L. C. Tribedi, Nucl. Instrum. Methods Phys. Res., Sect. B **267**, 157 (2014).
[37] Some parts of the picture are taken from http://hjklol.mit.edu/content/geometries-strings-smiles-and-openbabel and https://www.youtube.com/watch?v=R9cAzKQMSkA.
[38] A. N. Agnihotri, S. Nandi, S. Kasthurirangan, A. Kumar, M. E. Galassi, R. D. Rivarola, C. Champion, and L. C. Tribedi, Phys. Rev. A **87**, 032716 (2013).
[39] S. Biswas, D. Misra, J. M. Monti, C. A. Tachino, R. D. Rivarola, and L. C. Tribedi, Phys. Rev. A **90**, 052714 (2014).
[40] A. V. Verkhovtsev, A. V. Korol, and A. V. Solovyov, Phys. Rev. A **88**, 043201 (2013).
[41] T. LeBrun, H. G. Berry, S. Cheng, R. W. Dunford, H. Esbensen, D. S. Gemmell, E. P. Kanter, and W. Bauer, Phys. Rev. Lett. **72**, 3965 (1994).
[42] A. H. Kelkar, U. Kadhane, D. Misra, A. Kumar, and L. C. Tribedi, J. Phys. B: At., Mol. Opt. Phys. **40**, 2481 (2007).
[43] M. Ya. Amusia, L. V. Chernysheva, and E. Z. Liverts, Phys. Rev. A **85**, 042722 (2012).
[44] J. W. Cooper, Phys. Rev. A **42**, 6942 (1990).
[45] J. W. Cooper, Phys. Rev. A **47**, 1841 (1993).